

1  
2  
3  
4  
5  
6  
7  
8  
9  
10  
11  
12  
13  
14  
15  
16  
17  
18  
19  
20  
21  
22  
23  
24  
25  
26  
27  
28  
29  
30

Settling velocity spectra and the ballast ratio hypothesis

by

Robert A. Armstrong<sup>1,\*</sup>, Michael L. Peterson<sup>2,+</sup>, Cindy Lee<sup>1</sup>, and Stuart G. Wakeham<sup>3</sup>

<sup>1</sup>Marine Sciences Research Center, School of Marine and Atmospheric Sciences, Stony Brook University, Stony Brook, NY, USA

<sup>2</sup>School of Oceanography, University of Washington, Box 357940, Seattle, WA, USA

<sup>3</sup>Skidaway Institute of Oceanography, 10 Ocean Sciences Circle, Savannah, GA, USA

\*To whom correspondence should be addressed: [rarmstrong@notes.cc.sunysb.edu](mailto:rarmstrong@notes.cc.sunysb.edu)

+ Current address: Ocean Science Consulting and Research, 9433 Olympus Beach Road NE, Bainbridge Island, WA 98110

Submitted 05/18/2007; in revised form 07/14/2008; in re-revised form 10/03/08

Key words: settling velocity; ocean carbon cycle; POC; ballast; remineralization; fecal pellets; aggregates

## Abstract

31  
32  
33  
34  
35  
36  
37  
38  
39  
40  
41  
42  
43  
44  
45  
46  
47  
48  
49  
50  
51  
52  
53  
54  
55  
56  
57  
58  
59  
60  
61

Recently it has been observed that a strong quantitative relationship exists between asymptotic fluxes of Particulate Organic Carbon (POC) to the deep ocean and asymptotic fluxes of “ballast” minerals (opal; calcium carbonate; dust). It has further been suggested that this relationship might lead to a greater mechanistic understanding of POC transport, leading in turn to improved representations of remineralization in ocean carbon models. Since the depth scale of remineralization  $z^*$  is the ratio  $k / v$  of a remineralization rate  $k$  and a settling velocity (SV)  $v$ , a mechanistic understanding of settling velocities will be crucial in developing such models.

Historically, there have been two approaches to estimating the speed with which POC is transported to the deep ocean. First, settling speeds of single particles have been observed directly in both field and laboratory settings; estimates of fecal pellet sinking velocities tend to be higher and more variable than those of aggregates. Second, estimates have been made of the velocity at which temporal patterns in flux propagate between pairs of sediment traps separated in depth (the “benchmark approach”); recent studies have shown these results to be variable and to depend on mineral ballasting. Here we present SV estimates using a relatively new technology: Indented Rotating Sphere (IRS) sediment traps run in settling velocity (SV) mode. In this approach, particles are separated into SV classes during settling to collection cups. In MedFlux, SV data were collected concurrently with time-series (TS) data; the latter were used to construct benchmark estimates for comparison to the SV estimates. From the SV data, the range of modal settling velocities (sinking velocities having the largest time-averaged mass flux densities) in the fast-sinking fraction was estimated to be 287 – 503 m/d; the average of these modal values is 353 m/d, with standard deviation 76 m/d. In contrast, mean settling velocities of the fast-sinking fraction depend on the range of settling velocity classes included in the estimate. If only SV classes settling at  $> 50$  m/d are included, the range of SV’s at MedFlux was 214 – 298 m/d, with average mean value 242 m/d and standard deviation 31 m/d. These mean-velocity results are in excellent agreement with benchmark estimates of signal propagation velocities at Medflux ( $220 \pm 65$  m/d); they are also well within the range of other recent benchmark studies. The agreement between the benchmark estimates and mean settling velocity estimates at MedFlux, but not with modal velocities, argues that the benchmark method estimates mean velocities.

## 62 1. Introduction

63

64 It has long been known that minerals, both biogenic (opal; calcite; aragonite) and  
65 lithogenic (dust; riverine inputs), can increase the excess density of settling particles, which  
66 should in turn (all other things being equal) increase the settling velocity of Particulate Organic  
67 Carbon (POC) (Ittekkot and Haake, 1990; Honjo, 1996). However, only recently has it been  
68 proposed (Armstrong et al., 2002) that there is a strong quantitative relationship between POC  
69 fluxes and the fluxes of these “ballast” minerals, and that this relationship might lead to more  
70 accurate prediction of POC fluxes in ocean carbon models (e.g., Howard et al., 2006). In  
71 particular, Armstrong et al. (2002) and Klaas and Archer (2002) showed that while POC:ballast  
72 ratios were high and variable in the surface ocean, they converge to narrow ranges of values in  
73 the deep ocean (2.3 – 2.6 wt% carbon for opal ballast; 6.5 – 8.3 wt% C for carbonate and  
74 lithogenic ballasts; Klaas and Archer, 2002, their Table 2, “selected traps”). This relationship had  
75 been noted before: Deuser et al. (1981; their Fig. 9), for example, plotted the organic carbon  
76 content of the  $< 37 \mu\text{m}$  fraction of their samples versus total mass; their clearly significant  
77 regression indicated that the wt% organic carbon was 6 – 6.5%. However, this observation was  
78 made long before the era of large-scale ocean carbon simulations, and the importance of their  
79 finding was under-appreciated.

80 Understanding the mechanistic basis for observed patterns in POC:ballast ratios is of  
81 potentially great importance for understanding and predicting the ocean’s role in the global  
82 carbon cycle. Because calcium carbonate is both a major ballast mineral (François et al., 2002;  
83 Klaas and Archer, 2002) and the major route by which alkalinity is exported from the surface  
84 ocean, the ballast ratio hypothesis has implications for both global warming and global  
85 acidification (Feely et al., 2004). For example, Klaas and Archer (2002; their Table 2, depths  $>$   
86 2000 m) estimated that 1 gram (0.01 mol) of calcium carbonate carries with it  $\sim 0.072$  g (0.006  
87 mol) organic carbon, for a (molar) C:Ca export ratio of  $\sim 1.6$ . Since each calcium atom carries  
88 two positive charges, the depletion of alkalinity due to calcium export has a greater effect on pH  
89 and  $\text{pCO}_2$  than does the biological use and export of carbon, leading to acidification and to a  
90 decrease in the ocean’s ability to take up  $\text{CO}_2$  (Sarmiento and Gruber, 2006, p. 333). By  
91 contrast, carbon export ballasted by opal or dust, or not ballasted at all, causes no decrease in  
92 alkalinity, and hence a decline in  $\text{pCO}_2$ .

93           Klaas and Archer (2002) analyzed an extensive set of data from sediment traps. Using a  
94 multiple linear regression of POC fluxes on opal, calcium carbonate, and lithogenic fluxes, they  
95 were able to explain 85 – 90% of the variance in POC fluxes below 1000 m. This is an  
96 astonishing level of predictive power for an ocean biogeochemical model, and suggests (a) that  
97 most POC sinking below 1000 m is indeed ballasted (else ballast minerals would not predict  
98 POC flux nearly so well), and (b) that the mechanism or mechanisms responsible for these  
99 patterns must be capable of producing asymptotic convergence with depth.

100           This set of quantitative hypotheses has become known as the “ballast hypothesis.” We  
101 propose the more precise appellation “ballast ratio hypothesis” to emphasize that the hypothesis  
102 seeks to predict (asymptotic) POC:ballast flux ratios, and to differentiate it from the simpler (and  
103 long-accepted) observation that mineral ballasts promote sinking (Ittekkot and Haake, 1990;  
104 Honjo, 1996). The ballast ratio hypothesis does not say that ballasts are necessary for particle  
105 sinking: the experiments of Engel et al. (this volume) show clearly that unballasted particles can  
106 sink very rapidly if they are large enough ( $\geq 950$  m/d in their study). The hypothesis does state,  
107 however, that a large fraction of particles must be ballasted to the sea floor, at least in the present  
108 ocean, or the predictive power of ballast fluxes would not be so high.

109           Armstrong et al. (2002) proposed a model in which the POC:ballast ratio in the upper  
110 ocean is in excess of an asymptotic POC:ballast ratio, and where this “excess” POC is  
111 remineralized during descent to the abyss. They proposed two mechanisms that could keep  
112 remineralization from lowering POC:ballast ratios beyond an asymptotic limit: (i) that a certain  
113 fraction of POC is “protected” from remineralization through its physical association with  
114 mineral ballasts (analogous to the hypothesis of Mayer, 1994, for sediments); and/or (ii) that  
115 some minimum fraction of POC “glue” is needed to hold a sinking particle together in the face of  
116 sinking-generated shear (Hill, 1998); below this critical fraction, particles lose coherence, stop  
117 sinking, and so are not caught in sediment traps. Armstrong et al. (2002) modeled both  
118 postulated mechanisms by assuming that the POC pool consists of two fractions: a  
119 “quantitatively associated” fraction that is directly proportional to ballast mass, and an “excess”  
120 fraction that is remineralized during transit to the sea floor. (Note that Armstrong et al. used the  
121 term “quantitatively associated,” not “protected,” to accommodate both mechanisms.)

122           More recently, Passow and de la Rocha (2006) proposed that the concentration of POC,  
123 not the concentration of ballast, may at times limit the formation of sinking aggregates; in such

124 cases, sinking particles would be exported from the surface ocean at the asymptotic POC:ballast  
125 ratio, rather than converging to this ratio with depth.

126         Where glue is the limiting constituent (Passow and de la Rocha, 2006), the existence of  
127 an asymptotic POC:ballast ratio will certainly aid model predictions. However, we feel that  
128 ballast limitation is likely to prove more common than glue limitation. In this case, two factors  
129 will determine how useful asymptotic ballast ratios will be to model prediction: (i) if the ratio of  
130 excess POC to quantitatively associated POC is large, and/or (ii) if the depth scale of  
131 remineralization  $z^*$  is long, significant quantities of excess POC may survive to depth; in these  
132 cases, the existence of asymptotic POC:ballast ratios will not greatly aid model predictions.  
133 However, even if asymptotic ratios are not always useful, investigations of the ballast ratio  
134 hypothesis should lead to better mechanistic understanding of POC transport, which in turn  
135 should lead to improved representations of remineralization in ocean carbon models.

136         Historically there have been two approaches to estimating the speed with which POC is  
137 transported to the deep ocean. The first approach is direct observation of sinking particles in field  
138 and laboratory settings. In general, reported settling velocities of aggregates are low (e.g.,  $74 \pm$   
139  $39$  m/d, with range  $\sim 20$  m/d –  $\sim 200$  m/d: Alldredge and Gotschalk, 1988; “nonsinking” to  $30 -$   
140  $200$  m/d: Asper et al., 1992;  $\sim 21 \pm \sim 8$  m/d: Pilskaln et al., 1998) relative to those of sinking fecal  
141 pellets (e.g.,  $126 - 862$  m/d, with mean  $240$  m/d: Fowler and Small, 1972;  $\sim 20 - \sim 1000$  m/d:  
142 Komar et al., 1981).

143         The discrepancy between reported sinking velocities of aggregates and fecal pellets has  
144 led to some disagreement as to the “usual” range of settling velocities in the ocean. Some insight  
145 on this question can be gained from estimates made using a second major technique: the so-  
146 called “benchmark” method, in which the time-of-flight of a temporal pattern in flux abundance  
147 between traps separated in depth is estimated (Honjo, 1996). Benchmark estimates are not  
148 strictly “settling velocities” in the sense applied to direct observations; they are more properly  
149 “signal propagation velocities,” and may represent some sort of average over several settling  
150 velocity classes. Early estimates of signal transport centered on the range  $80 - 200$  m/d (Honjo,  
151 1996). However, more recent results from studies using the benchmark approach suggest a more  
152 variable range and a somewhat higher mean.

153         In a pioneering study, Müller and Fischer (2001) applied the benchmark method to  
154 alkenone fluxes from the Cape Blanc region of the eastern Atlantic. They estimated low

155 propagation velocities (63 – 88 m/d) during periods of low alkenone flux, but high propagation  
156 velocities ( $\geq 280$  m/d) during a period of high alkenone flux; since alkenones are tracers of  
157 coccolithophids, they attributed this difference to low ballasting by coccolithophorids when  
158 alkenone concentrations were low and high ballasting when alkenones were high. A recent study  
159 by Ploug et al. (2008) gives added support to the importance of ballast minerals. Ploug et al.  
160 compared settling velocities of fecal pellets produced by the copepod *Temora longicornis* when  
161 fed on diets of the nanoflagellate *Rhodomonas* sp., the diatom *Thalassiosira weissflogii*, or the  
162 coccolithophorid *Emiliana huxleyi*; settling velocities were  $35 \pm 29$  m/d,  $322 \pm 169$  m/d, and  
163  $200 \pm 93$  m/d, respectively, on the three diets, clearly demonstrating the importance of ballast  
164 for fecal pellet settling velocities.

165 Berelson (2002) used correlations among a suite of tracer ratios to estimate propagation  
166 velocities for U.S. JGOFS studies in the equatorial Pacific (EqPac) and the Arabian Sea (ASPS).  
167 For these studies, Berelson (2002) found settling velocities of  $211 \pm 79$  m/d, higher than the  
168 canonical range 80 – 200 m /d, despite the fact that his estimates were biased low (Xue and  
169 Armstrong, this volume). And again despite this bias, 11 of 18 of Berelson’s propagation  
170 velocity estimates were  $\geq 200$  m/d.

171 Fischer et al. (2007) used both the pure benchmark method (“major peak method”) and  
172 Berelson’s correlation method to estimate propagation velocities at several locations in the  
173 Atlantic Ocean. Their estimates spanned a large range (60 – 750 m/d); both methods produced  
174 SV estimates that were  $> 200$  m/d at 7 of 15 sites.

175 Finally, in a companion paper in this volume, Xue and Armstrong used an improved  
176 benchmark method to estimate settling velocities using MedFlux data plus data from U.S.  
177 JGOFS process studies. Their estimated propagation velocity was  $220 \pm 65$  m/d for 3 MedFlux  
178 trap pairs and  $205 \pm 74$  m/d for 15 “high resolution” trap pairs (cup rotation times  $\leq 8.5$  d) from  
179 MedFlux and the JGOFS Arabian Sea Process Study.

180 The MedFlux data used by Xue and Armstrong (this volume) were obtained using  
181 Indented Rotating Sphere (IRS) sediment traps deployed in time-series (TS) mode (Peterson et  
182 al., 1993). During MedFlux, IRS traps were also deployed in Settling Velocity (SV) mode. These  
183 SV data are used in the present paper to provide independent estimates of settling velocity at  
184 MedFlux; comparison of the present study to results from Xue and Armstrong also yields  
185 valuable clues as to what the benchmark method may actually measure. In particular, does the

186 signal detected by the benchmark method correspond to the settling velocity of the SV class with  
 187 the largest flux density (the “modal” velocity)? Or does it correspond more closely to some sort  
 188 of mean (average) settling velocity, perhaps also where only particles sinking faster than some  
 189 minimum velocity should be included in the average?

190 In the following sections, we first discuss how modal (most likely) and mean (average)  
 191 settling velocities can be estimated from IRS SV data. We then present settling velocity  
 192 estimates and relate them to the results from Xue and Armstrong (this volume) and other studies.

193

## 194 2. Materials and Methods

195

### 196 2.1. Indented Rotating Sphere (IRS) sediment traps in settling velocity (SV) mode: basic 197 considerations

198

199 Indented Rotating Sphere (IRS) sediment traps can be used either to record a time-series  
 200 of sinking fluxes (Time-Series (TS) mode: Peterson et al., 1993; Lee et al., this volume; Xue and  
 201 Armstrong, this volume) or to separate fluxes into settling velocity classes (Settling Velocity  
 202 (SV) mode: Peterson et al., 2005, and this volume). The novel feature of the IRS design is an  
 203 indented spherical valve, or ball, that rotates to allow particles to enter the settling chamber while  
 204 (largely) excluding swimmers (Peterson et al., 1993, 2005). Each trap has 12 collection  
 205 positions: position 1 is opened during deployment and recovery, and positions 2 – 12 have cups  
 206 that collect samples. In SV mode, the valve is rotated once per day, at which time material that  
 207 has accumulated on the ball is deposited into a settling chamber. Over the next 24 hours, the 11  
 208 collection cups are rotated on a fixed schedule (see Table 1); the most rapidly sinking material is  
 209 collected in the first collection cup, slower-sinking material in the next cup, and so forth. The  
 210 result is a collection of particles that have been separated based on the length of time taken to  
 211 traverse the settling chamber. Settling velocities are then estimated by assuming that the time  $t$   
 212 (days) taken for a sinking particle to traverse the settling chamber (0.68 m in length) is inversely  
 213 proportional to its settling velocity ( $SV$ ):

214

$$215 \quad SV \text{ (m d}^{-1}\text{)} = 0.68 / t . \quad (1)$$

216

217 Of greater utility is the logarithmic form of Eq. (1):

218

$$219 \quad \log_{10}(SV) = \log_{10}(0.68) - \log_{10}(t) . \quad (2)$$

220

221 These relationships are fundamental, because the data collected by SV traps are masses caught in  
 222 time intervals (since the last ball rotation) when particular cups were open (Table 1), whereas  
 223 SV's are the quantities of most direct biogeochemical interest.

224 Data were collected at the French JGOFS DYFAMED site in the Ligurian Sea ~52 km  
 225 off Nice (43° 20' N, 7° 40' E) in ~2300 m of water. In these studies, each IRS frame held three  
 226 traps: two SV traps ("SV1" and "SV2") and one time-series (TS) trap. Both SV records are  
 227 available from deployments at 238 m in March-May 2003, the deployment at 117 m in May-June  
 228 2003, and deployments at 524 m and 1918 m in February-April 2005. (Deployment dates and  
 229 intervals are given in the legends to Figs. 1 and 2. Also see Table 2 for a summary of results.) In  
 230 the May-June 2003 deployment, fluxes were so low that samples from the two SV traps were  
 231 combined before filtering and were analyzed together, so that only a single data record was  
 232 created. In the 313 m 2005 deployment, trap SV1 trapped a large amount of black material from  
 233 an unknown source, compromising the samples; therefore, only results from SV2 are reported.

234

## 235 2.2. Plotting the data, and the need for normalizing by settling velocity interval (SVI)

236

237 Data were plotted as histograms (Figs. 1 and 2) on logarithmic ( $\log_{10}$ ) scales of settling  
 238 velocity. Denote by  $M_{total}$  the total mass (mg) collected in all the cups during a deployment, and  
 239 by  $M_i$  the mass caught in cup  $i$ ; both measurements are standardized to a collection area of 1  
 240  $m^2$ , giving the  $M$ 's units of  $mg/m^2$ . Dividing these masses by the total length of the deployment  
 241 period  $T$  gives time-averaged mass fluxes  $\overline{MF}$  ( $mg/m^2/d$ ). The total area of the associated  
 242 histogram (see Figs. 1 and 2) represents  $\overline{MF}_{total}$ , and the area of histogram element (rectangle)  $i$   
 243 represents the mass flux  $\overline{MF}_i$  in SV class  $i$ . To calculate the height of each rectangle, the time-  
 244 average mass fluxes  $\overline{MF}_i$  are divided by the length of the base of the rectangle (the "settling  
 245 velocity interval"  $SVI_i$ ):

246

247 
$$SVI_i = \log_{10}(t_{i,close}) - \log_{10}(t_{i,open}) , \quad (3)$$

248

249 where  $t_{i,open}$  and  $t_{i,close}$  are times (since the last ball rotation) that cup  $i$  opened or closed,

250 respectively (see Table 1). Substituting Eq. (2) into Eq. (3) yields

251

252 
$$SVI_i = \log_{10}(SV(t_{i,open})) - \log_{10}(SV(t_{i,close})) . \quad (4)$$

253

254 Settling velocity intervals are not needed in most data-fitting applications, because in  
 255 most applications intervals along the  $x$ -axis are either chosen to be of equal lengths, or the  $x$ -axis  
 256 is taken to be continuous. In the present application, due to instrumental limitations, not all size  
 257 classes could be made of equal length along an axis of  $\log_{10}(SV)$ , and SV classes with larger  
 258 SVI's will collect more mass. In the present study, the most striking example (see Table 1) is in  
 259 2005, where SV cup 6 has an SVI of  $\log_{10}(7/5) \approx 0.146$  while the SVI of SV cup 12 is  
 260  $\log_{10}(1440/180) \approx 0.903$ . If these two size classes had the same intensity of particle delivery, we  
 261 would expect cup 12 to receive more than 6 times as much material as cup 6; conversely, if cup 6  
 262 received 0.146 mg/d, and cup 12 received 0.903 mg/d, by correcting for SVI we could see that  
 263 both were experiencing the same intensity of particle interception. This correction therefore  
 264 allows us to interpret ratios of histogram heights as ratios of delivery intensities.

265 Below and in Figs. 1 and 2, the heights of histogram elements  $\overline{MFD}_i = \overline{MF}_i / SVI_i$  will  
 266 be called “time-averaged mass flux densities”: they are “mass fluxes” ( $\text{mg}/\text{m}^2/\text{d}$ ) “averaged”  
 267 over the deployment time, and become “densities” (in the sense of probability densities) when  
 268 divided by their SVI's (final units:  $\text{mg}/\text{m}^2/\text{d}/\text{SVI}$ ).

269 For the fastest SV class,  $t_{open} = 0$ , leading to an infinite SVI. In this case, we have  
 270 arbitrarily used a value  $t_{open} = 0.5$  min in plotting the data. This problem is only cosmetic,  
 271 however, and does not affect the data-fitting procedure, where the data have been fit using  
 272 cumulative distributions.

273

274

275

276 2.3. Estimating modal sinking velocities

277

278 A two-part model was fit to the data. First, it is evident from Figs. 1 and 2 that the  
 279 distribution of the fast-sinking fraction of the flux is close to Gaussian on a logarithmic scale of  
 280 settling velocity. However, to allow estimation of modal settling velocities of these Gaussian  
 281 portions, which dominate sinking fluxes, they must be separated from the long “tail” of slow-  
 282 sinking particles. To accomplish this separation, we have postulated an exponential model for the  
 283 slow-sinking tail, and have fit the sum of the Gaussian and exponential models to the data. (Note:  
 284 for a Gaussian distribution, the mean, mode, and median are equal; however, since only the  
 285 mode remains invariant upon logarithmic transformation, we will refer to the highest point on the  
 286 Gaussian curve as its mode.)

287 First, the distribution of mass flux density associated with the Gaussian part can be  
 288 written

289

$$290 \quad \phi_{Gauss}(SV) = \frac{\overline{MFD}_{Gauss}}{\sqrt{2\pi\sigma_{Gauss}^2}} \exp\left(-\frac{(\log_{10}(SV) - \log_{10}(SV_{mode}))^2}{2\sigma_{Gauss}^2}\right), \quad (5)$$

291

292 where  $SV_{mode}$  is the mode and  $\sigma_{Gauss}^2$  is the variance of the distribution. (This variance is on a  
 293  $\log_{10}$  scale of SV; it is therefore dimensionless.) However, from Eq. (2), note that

294

$$295 \quad (\log_{10}(SV) - \log_{10}(SV_{mode}))^2 = (\log_{10}(t) - \log_{10}(t_{mode}))^2, \quad (6)$$

296

297 so that Eq. (5) can also be written in terms of time  $t$  (days) since the last valve rotation:

298

$$299 \quad \phi_{Gauss}(t) = \frac{\overline{MFD}_{Gauss}}{\sqrt{2\pi\sigma_{Gauss}^2}} \exp\left(-\frac{(\log_{10}(t) - \log_{10}(t_{mode}))^2}{2\sigma_{Gauss}^2}\right). \quad (7)$$

300

301 Second, the “tail” of slow-sinking particles is modeled by assuming that it is generated by  
 302 an exponential decay of mass into whatever cup happens to be open at a given time; since cups

303 collecting slower-sinking particles are open for longer times, they tend to collect more of the  
 304 slower-sinking fraction. In particular, if a mass  $M_{slow}$  of slow-sinking detritus is introduced into  
 305 the sinking chamber following a particular valve rotation (call this time  $t = 0$ ), then the rate of  
 306 transfer  $R(t)$  of this mass into the *SV* cup that is open at time  $t$  (days) will be

$$307 \quad R(t) = M_{slow} k_{slow} \exp(-k_{slow} t), \quad 0 < t < \infty, \quad (8)$$

308

309 where  $k_{slow}$  ( $d^{-1}$ ) is a decay rate.

310 Eq. (8) embodies the notion that a certain fraction of the slow-settling particles from a  
 311 given rotation will still be in the settling chamber at the time of the next rotation. However, since  
 312 the cups rotate every 24 hr, the particles that sink out at  $t + 1, t + 2, \dots, t + n$ , etc., will go into  
 313 the same cup as those that sank out at time  $t$ . Taking this periodicity into account, and assuming  
 314 that  $k_{slow}$  is constant over the deployment interval, the exponential part  $\phi_{slow}(t)$  becomes

315

$$316 \quad \phi_{slow}(t) = \overline{M}_{slow} k_{slow} \sum_{n=0}^{\infty} \exp(-k_{slow}(t+n)) \quad (9)$$

$$= \overline{M}_{slow} \frac{k_{slow} \exp(-k_{slow} \times t)}{1 - \exp(-k_{slow} \times 1)}, \quad 0 < t < 1.$$

317

318 To avoid the problem of infinite *SV* for the fastest-sinking size class (Section 2.2), fluxes  
 319 were fit to the data using cumulative functions (the integrals of Eqs. 7 and 9) over the interval  $(0$   
 320  $< t < 1)$  (d). These functions were fit by maximizing a likelihood statistic with Gaussian errors  
 321 (Edwards, 1992; Hilborn and Mangel, 1997); the estimator used was

322

$$323 \quad \ln(L) = -(n/2) \ln \sum_{j=1}^8 \sum_{i=1}^{11} \left( \left( \overline{MF}_{ji} / \overline{MF}_{j,total} \right)_{data} - \left( \overline{MF}_{ji} / \overline{MF}_{j,total} \right)_{model} \right)^2. \quad (10)$$

324

325 In Eq. (10),  $j$  indexes the 8 *SV* trap records and  $i$  indexes the 11 cups within each record; the total  
 326 number of data points was therefore  $n = 88$ . Parameter estimates from these fits are shown in  
 327 Table 2.

328 To allow visual comparison of the fits to the data, the fitted curves were added to the  
 329 histogram plots (Fig. 1 for the data from 2003; Fig. 2 for 2005). In these plots the exponential tail  
 330 model (Eq. 9) does not look exponential, because it is exponential on a linear scale of time  $t$ , not  
 331 on scale of  $\log_{10}(SV)$ ; that is, because, using the natural logarithmic form of Eq. (2),

$$\begin{aligned}
 \exp(-k_{slow}t) &= \exp(-k_{slow}e^{\ln(t)}) \\
 &= \exp(-k_{slow}e^{\ln(0.68)-\ln(SV)}) \\
 &= \exp(-0.68k_{slow}e^{-2.3\log_{10}(SV)}) .
 \end{aligned}
 \tag{11}$$

334

#### 335 2.4. Calculating mean settling velocities

336

337 A time-averaged mass flux density  $\overline{MFD}_i$  (mg/m<sup>2</sup>/d/SVI) is the product of a sinking  
 338 velocity  $SV_i$  (m/d) and a time-averaged mass concentration density  $\overline{MCD}_i$  (mg/m<sup>3</sup>/SVI); the  
 339 (unknown) values of the  $\overline{MCD}_i$  can therefore be calculated as

340

$$\overline{MCD}_i = \overline{MFD}_i / SV_i .
 \tag{12}$$

342

343 Note particularly that the estimated concentration densities  $\overline{MCD}_i$  are those *in the water column*  
 344 *outside the trap*; that is, they are the mass concentration densities that *gave rise to* the observed  
 345 mass flux densities (cf. Asper et al., 1992). In Eq. (12), the average sinking velocities within  
 346 intervals are estimated as the average  $\log_{10}(SV)$  at the beginning and end of the interval, which  
 347 is identical to the geometric mean of the SV's themselves; that is, we take  $SV_i$  to be

348

$$SV_i = \sqrt{SV(t_{i,open}) SV(t_{i,close})} .
 \tag{13}$$

350

351 Estimated distributions of  $\overline{MCD}_i$  for the eight MedFlux deployments are shown in Fig. 3.

352 Average sinking velocity of total mass is next defined in the usual manner by weighting  
 353 the settling velocity in each SV class by its mass concentration density; that is, we compute

354

$$SV_{avg} = \frac{\sum_{i=i_{min}}^{11} \overline{MCD}_i \cdot SV_i}{\sum_{i=i_{min}}^{11} \overline{MCD}_i} = \frac{\sum_{i=i_{min}}^{11} \overline{MFD}_i}{\sum_{i=i_{min}}^{11} \overline{MFD}_i / SV_i} . \quad (14)$$

356

357 In Eq. (14), the summation is allowed to vary with  $i_{min}$ , the index of the slowest settling velocity  
 358 class that is included in the summation. Results are plotted in Fig. 4 and summarized in Table 3.  
 359 Minimum SV's for each cup in 2003 and 2005 are given in Table 1. In Fig. 4, average SV's are  
 360 plotted against the smallest SV in the summation. In Table 3, the minimum settling velocity  
 361 included in the summation was taken to be 50 m/d, the visual location of the crossover point  
 362 between the Gaussian peak and exponential tail in Figs. 1 and 2; correspondingly, in 2003, cups  
 363 2 – 6 were included in the average, and in 2005, cups 2 – 8.

364

### 365 3. Results

366

#### 367 3.1. Modal settling velocities

368

369 Estimated settling velocity spectra are displayed in Figs. 1 and 2; estimated parameter  
 370 values are listed in Table 2. The overall pattern is one of a Gaussian distribution of fast-settling  
 371 particles that accounts for 62 – 77% of the mass flux (Table 2), plus an exponential “tail” of  
 372 slow-sinking particles that accounts for the remaining 23 – 38%. Modal settling velocities of the  
 373 fast-sinking fraction (Table 2) were 287 – 503 m/d; the mean of these modal values is 353 m/d,  
 374 with standard deviation 76 m/d (Table 3).

375

376 One remarkable result is that the shape of the settling velocity spectrum was virtually  
 377 constant over 5 deployments spanning two years (2003 and 2005), two seasons within 2003, and  
 378 3 depths in 2005 (Fig. 5). Since 7 of 8 MedFlux deployments took place in late-winter/early-  
 379 spring, restricted sampling of seasonality may therefore have contributed substantially to the  
 380 similarity of these SV distributions.

380

381 A second important result is that the differences among traps on the same frame, only  
 382 centimeters apart, are comparable in magnitude to differences between years (Tables 2 and 3).

382

Trap-to-trap variability in both modal settling velocity ( $SV_{mode}$ ) and in the variance  $\sigma_{Gauss}^2$  of the

383 fast-settling (Gaussian) component of the flux is as large (or larger) between traps deployed on  
 384 the same frame (March-May 2003, and 524 m and 1918 m in 2005) than it is among depths or  
 385 between years. This observation argues that noise in the trapping process may require large  
 386 sample sizes to resolve patterns related to depth, season, or year.

387 A third important pattern (Table 2) is that variation among individual traps in shape of  
 388 the tail distributions of fairly small, as shown by the narrow ranges of the tail parameters  $f_{Gauss}$   
 389 and in  $k_{slow}$ ; the former range from 0.267 to 0.360, and the latter from  $3.01 \text{ d}^{-1}$  to  $5.23 \text{ d}^{-1}$  for  
 390 all periods except May-June 2003. Over one day,  $\exp(-3.01) = 0.049$  and  $\exp(-5.23) = 0.0054$ ,  
 391 so that between 95% and 99.5% of the slow-sinking flux is predicted to clear from the settling  
 392 tube in one day. However, the clearance rate in May-June 2003 is several times smaller than in  
 393 other deployments, with  $\exp(-1.18) = 0.30$ , so that only 70% is cleared in any one cycle. This  
 394 observation may be related to the fact that the flux in May-June 2003 was an order of magnitude  
 395 smaller than in any other observation period.

396

### 397 3.2. Mean settling velocities

398

399 Mean settling velocities for fast-settling particles (SV's  $> 50 \text{ m/d}$ ; see Section 2.4 and  
 400 Fig. 4) were notably lower than modal velocities; their range is 214 – 298 m/d, with average  
 401 mean value 242 m/d and standard deviation 31 m/d (Table 3). The difference between modal and  
 402 mean settling fluxes is can be seen by considering Eq. (12): if particles of two SV's have the  
 403 same flux (as recorded by the masses in their respective cups), the mass concentration outside the  
 404 trap must be higher for the slower-sinking particles (see Eq. 12); slower-sinking particles are  
 405 therefore weighted more heavily than fast-sinking particles in calculating mean SV's.

406

## 407 4. Discussion

408

409 We have here presented two sets of results from IRS sediment traps run in settling  
 410 velocity (SV) mode. First we showed settling velocity spectra (Figs. 1 and 2, and Table 2) from  
 411 these traps. The spectra from MedFlux all have a common shape: a Gaussian portion of “fast-  
 412 settling” particles that explain 62 – 77% of the mass flux; and an exponential “tail” that explains

413 23 – 38% of the flux. Our estimate of modal settling velocities (velocities having the highest  
414 mass flux densities; the peak of the Gaussian part of the spectrum) is  $353 \pm 76$  m/d.

415 We have also presented results for mean settling velocities of the fast-settling particles.  
416 Since mean values depend on the range of SV's included (Eq. 14 and Fig. 4), we have taken the  
417 value at the boundary of the Gaussian and exponential SV spectra (50 m/d) as the lowest SV to  
418 be included in our best estimate of mean SV's. Mean velocities were notably lower than modal  
419 velocities; their range (for SV's > 50 m/d) is 214 – 298 m/d, with average mean value 242 m/d  
420 and standard deviation 31 m/d (Table 3). Both sets of results are noticeably higher than the range  
421 80 – 200 m/d (Honjo, 1996) that is widely accepted as “typical” by the oceanographic  
422 community, and also higher than the values typically found in studies of sinking aggregates (see  
423 the Introduction). However, both sets are well within the range of values obtained from results  
424 on sinking fecal pellets.

425 Direct evidence for the dominant role of fecal pellets at MedFlux is provided by studies  
426 of the chemical properties of the samples. Wakeham et al. (this volume) found that MedFlux  
427 samples were typically characterized both by large fluxes of diatom pigments and by compounds  
428 characteristic of extensive zooplankton degradation. In addition, Abramson (2007) found very  
429 little interaction between sinking particles and suspended particles; this finding is in direct  
430 contrast to the model of Asper et al. (1992) for sinking aggregates, where the interaction of  
431 sinking aggregates with nonsinking aggregates was posited to be the driving force for sinking to  
432 the sea floor. Finally, during the turnaround of the traps in May 2003 we observed a large salp  
433 bloom, which could have produced fast-sinking fecal pellets. We conclude that mass fluxes at  
434 MedFlux were probably dominated by zooplankton-produced fecal pellets, not by aggregates,  
435 and therefore that both the SV results of the present paper and the TS results of Xue and  
436 Armstrong (this volume) are well within expected ranges.

437 Nevertheless, since the IRS/SV traps are a relatively new technology, we feel obliged to  
438 address some criticisms that might be directed at their use. It is possible, for example, that the  
439 IRS trap in SV mode introduces biases, perhaps due to aggregation or collapse of aggregates on  
440 the IRS valve. One piece of evidence against this proposition is that the flux spectrum for May-  
441 June 2003 is virtually identical to the other spectra, despite having a flux that is an order of  
442 magnitude lower than the others; if aggregation had been occurring, we would have expected  
443 substantially less aggregation at this lower flux. A second bit of evidence against substantial

444 alteration of particles on the IRS valve is that mean SV's from the SV traps are not substantially  
445 higher than the 220 m/d reported by Xue and Armstrong (this volume) for MedFlux time-series  
446 (TS) traps, or for MedFlux and U.S. JGOFS TS traps with high-resolution data (205 m/d). The  
447 MedFlux data used by Xue and Armstrong are from IRS traps used in Time Series (TS) mode.  
448 These data are immune to possible biases associated with particle alteration, because in TS mode  
449 the IRS valve is rotated frequently, and the collected sediment is deposited in whichever cup is  
450 open at the time. Since in TS mode particles are not sorted by settling velocity, it simply does not  
451 matter whether they aggregate or deflate while on the valve.

452 Another possible concern is that the Medflux SV distributions in Fig. 5 are all so similar,  
453 suggesting that they might have been produced artifactually. As evidence against this hypothesis,  
454 data from the North Pacific IRS/SV studies of Trull et al. (2008) and our MedFlux studies are  
455 presented together (Fig. 6). The three MedFlux traps are from depths comparable to those in the  
456 VERTIGO deployments at ALOHA and K-2; they present the same data presented as cumulative  
457 distributions in Fig. 6 of Trull et al. (2008), but have been plotted as histograms after  
458 normalization as described in Section 2.2 of the present paper and in the legend to Fig. 5. The  
459 most notable features of this comparison are (1) that the flux density peaks in the two studies do  
460 not occur at the same SV's, and (2) that the "tails" of the distributions are completely different.  
461 First, both VERTIGO K-2 peaks occurred at 141 m/d, the ALOHA peak was at 200 m/d, and the  
462 MedFlux peaks were at 310, 310, and 400 m/d. The ALOHA peak was therefore shifted one cup  
463 slower than the closest MedFlux peaks, and the K-2 peaks were both shifted 2 cups slower than  
464 the closest MedFlux peak. In addition, the ALOHA and K-2 peaks (Fig. 6) are outside the range  
465 of all MedFlux peaks (253 – 692 m/d; see Fig. 5). Second, and even more striking, while the tails  
466 of the MedFlux distributions all have the same characteristic shape (Fig. 5), the VERTIGO  
467 ALOHA distribution was enhanced in fast-sinking particles (relative to MedFlux) and the K-2  
468 peaks were enhanced in slow-sinking particles. These results show that the IRS SV traps do not  
469 always produce the same pattern due to artifacts in their design and/or deployment.

470 The differences noted above may indicate real differences among sites, or they may  
471 reflect other differences in deployment. The Medflux traps were deployed for periods of 47 – 61  
472 days, long enough that in most cases they averaged over bloom and non-bloom conditions; this  
473 averaging might lead to Gaussian distributions of fast-settling particles by the summing of  
474 several semi-independent processes (by the Central Limit Theorem of statistics). In contrast, the

475 VERTIGO traps were each deployed for 6 days, limiting the amount of averaging. The relative  
476 importances of site, season, and deployment length can only be assessed by more extensive  
477 trapping in SV mode.

478         The present results, combined with concurrent measurements of C:ballast ratios (Lee et  
479 al., this volume), may have significant implications for the ballast ratio hypothesis. From Figs. 7  
480 and 9 and Table 4 of Lee et al., it is clear that C:ballast ratios measured in near-surface traps  
481 have not declined to the 3 – 8% asymptotic value found by Klaas and Archer (2002), either by  
482 middepth (~300 – 500 m) or deeper (~1900 m). These measurements imply that “excess carbon”  
483 is not being remineralized as fast as with depth as predicted by the ballast ratio hypothesis.

484         We offer two explanations for this finding. First, mean SV’s at DYFAMED tend to be  
485 high (~220 – 240 m/d), and the deepest MedFlux trap was only at ~1900 m.; it is possible that a  
486 transit time of only 8 d may not be sufficient to allow for decay of C:ballast ratios to their  
487 asymptotic values. A more probable explanation is that there is a marked seasonality in C:ballast  
488 ratios, and that the late-winter/early-spring period, when the spring bloom occurs and most  
489 carbon is exported, has higher C:ballast ratios than those in much of the remainder of the year.  
490 This speculation would imply that C:ballast ratios at depth may owe much of their “constancy”  
491 to averaging over yearly cycles.

492         The distribution of particle settling velocities is of primary importance in the cycles of  
493 carbon and other elements in the ocean, since these spectra determine the depth distributions of  
494 organic matter remineralization and mineral dissolution. The realization that we are dealing with  
495 sinking velocity spectra, not single sinking velocities, requires that we start to think about the  
496 mechanisms that create and maintain these spectra; understanding these processes will be critical  
497 for predicting how the oceans will respond to global change.

498         We end by speculating on the relationship between mean settling velocity and modal  
499 settling velocity. First, visual inspection of the data (Fig. 5) and parameter estimates (Table 2)  
500 suggest that there is little change with depth in either the modal sinking velocity or in the width  
501 (variance) of the Gaussian peak. This seems a bit odd, as one might expect that the variance of  
502 the Gaussian envelope would increase with depth, as faster-sinking particles get farther ahead  
503 and slower-sinking particles lag farther behind. One possibility is that this casual observation is  
504 incorrect, and that the Gaussian fraction actually does spread out with depth. A second  
505 possibility is that the spectra all look similar because they are all taken at the same site, during

506 the same season, and with long (47 – 61 d) deployments. A more intriguing possibility is that  
507 sinking particles interact in such a way that the wave of sinking materials retains its shape;  
508 sinking material may therefore travel as solitary wave packets, or “solitons.” Although the most  
509 abundant (“modal”) settling velocity class moves at ~350 m/d, the wave packet as a whole seems  
510 to move much more slowly (220 – 240 m/d), more in line with (but still faster than) the canonical  
511 range 80 – 200 m/d (Honjo, 1996).

512

513

514

515

516

517

518

519

520

521

522

523

524

525

526

527

528

529

530

531

532

533

534

535

536

## 537 Acknowledgements

538

539 This work was partially funded by grants from the US National Science Foundation program in  
540 chemical oceanography. We also thank the International Atomic Energy Agency (IAEA) in  
541 Monaco for ship and materials support – especially when shipping and mooring problems  
542 occurred on the 2003 cruise – and for supporting our IAEA collaborators. The IAEA is in turn  
543 grateful for the support provided to its Marine Environmental Laboratory by the Government of  
544 the Principality of Monaco. This is MedFlux contribution #22, and contribution #1361 from the  
545 School of Marine and Atmospheric Sciences, Stony Brook University.

546

547

548

549

550

551

552

553

554

555

556

557

558

559

560

561

562

563

564

565

566

567

568

569

570

571

572

## 573 Literature Cited

- 574
- 575 Abramson, L. 2007. Mechanisms of mineral protection of organic matter in the water column.  
576 Ph.D. Dissertation. Stony Brook University, Stony Brook, NY, 179 pp.
- 577 Alldredge, A.L., Gotschalk, C., 1988. In situ settling behavior of marine snow. *Limnol.*  
578 *Oceanogr.* 33, 339-351.
- 579 Armstrong, R.A., Lee, C., Hedges, J.I., Honjo, S., Wakeham, S., 2002. A new, mechanistic  
580 model for organic carbon fluxes in the ocean based on the quantitative association of  
581 POC with ballast material. *Deep-Sea Res. II* 49, 219-236.
- 582 Asper, V.L., Honjo, S., Orst, T.H., 1992. Distribution of transport of marine snow aggregates in  
583 the Panama Basin. *Deep-Sea Res.* 39, 939-952.
- 584 Berelson, W.M., 2002. Particle settling rates increase with depth in the ocean. *Deep-Sea Res. II*  
585 49, 237-251.
- 586 Deuser, W.G., Rost, E.H., Anderson, R.F., 1981. Seasonality in the supply of sediment to the  
587 deep Sargasso Sea and implications for the rapid transfer of matter to the deep ocean.  
588 *Deep-Sea Res.* 28, 495-505.
- 589 Edwards, A.W.F., 1992. *Likelihood*. Johns Hopkins University Press, Baltimore, MD.
- 590 Engel, A., Szlosek, J., Abramson, L., Liu, Z., Stewart, G., Hirschberg, D., Lee, C. Investigating  
591 the effect of ballasting by CaCO<sub>3</sub> in *Emiliana huxleyi* I. Formation, settling velocities,  
592 and physical properties of aggregates (this volume)
- 593 Feely, R.A., Sabine, C.L., Lee, K., Berelson, W., Kleypas, J., Fabry, V.J., Millero, F.J., 2004.  
594 Impact of anthropogenic CO<sub>2</sub> on the CaCO<sub>3</sub> system in the oceans. *Science* 305, 362-  
595 366.
- 596 Fischer, G., Karakas, G., Blaas, M., Ratmeyer, V., Nowald, N., Schlitzer, R., Helmke, P.,  
597 Davenport, R., Donner, B., Neuer, S., Wefer, G., 2007. Mineral ballast and particle  
598 settling rates in the coastal upwelling system off NW Africa and the South Atlantic. *Int. J.*  
599 *Earth Sci.* DOI 10.1007/s00531-007-0234-7.
- 600 Fowler, S.W., Small, L.F., 1972. Sinking rates of euphausiid fecal pellets. *Limnol. Oceanogr.* 17,  
601 293-296.

- 602 François, R., Honjo, S., Krishfield, R., Manganini, S., 2002. Factors controlling the flux of  
603 organic carbon to the bathypelagic zone of the ocean. *Global Biogeochem. Cycles* 16,  
604 GB1087.
- 605 Hilborn, R., Mangel, M., 1997. *The ecological detective: confronting models with data.*  
606 Princeton Univ. Press, Princeton NJ, USA.
- 607 Hill, P.S., 1998. Controls on floc size in the coastal ocean. *Oceanography* 11, 13-18.
- 608 Honjo, S., 1996. Fluxes of particles to the interior of the open oceans. *p.* 91-154 *in* Particle Flux  
609 in the Ocean, SCOPE Vol. 57, Ittekkot, V., Schäfer, P., Honjo, S., Depetris, P.J., eds.  
610 John Wiley & Sons, New York.
- 611 Howard, M.T., Winguth, A.M.E., Klaas, C., E. Maier-Reimer, E., 2006. Sensitivity of ocean  
612 carbon tracer distributions to particulate organic flux parameterizations. *Global*  
613 *Biogeochem. Cycles* 20, GB3011.
- 614 Ittekkot, V., and Haake, B., 1990. The terrestrial link in the removal of organic carbon. *p.* 319-  
615 325 *in* Facets of Modern Biogeochemistry, Ittekkot, V., Kempe, S., Michaelis, W., Spitzky,  
616 A, eds. Springer, Berlin.
- 617 Klaas, C., Archer, D.E., 2002. Association of sinking organic matter with various types of  
618 mineral ballast in the deep sea: Implications for the rain ratio. *Global Biogeochem.*  
619 *Cycles* 16, 1116 doi:10.1029/2001GB001765.
- 620 Komar, P.D., Morse, A.P., Small, L.F., Fowler, S.W., 1981. An analysis of sinking rates of  
621 natural copepod and euphausiid fecal pellets. *Limnol. Oceanogr.* 26, 172-180.
- 622 Lee, C., Peterson, M.L., Wakeham, S.G., Armstrong, R.A., Cochran, J.K., Miquel, J.-C., Fowler,  
623 S., Hirschberg, D., Beck, A., Xue, J., Particulate organic matter and ballast fluxes  
624 measured using in time-series and settling velocity sediment traps in the northwestern  
625 Mediterranean Sea (this volume)
- 626 Mayer, L.M., 1994. Surface area control of organic carbon accumulation in continental shelf  
627 sediment. *Geochim. Cosmochim. Acta* 58, 1271-1284.
- 628 Müller, P.J., Fischer, G., 2001. A 4-year sediment trap record of alkenones from the filamentous  
629 upwelling region off Cape Blanc, NW Africa and a comparison with distributions of  
630 underlying sediments. *Deep-Sea Res. I* 48, 1877-1903.
- 631 Passow, U., de la Rocha, C.L., 2006. Accumulation of mineral ballast on organic aggregates.  
632 *Global Biogeochem. Cycles* 20, GB1013, doi:10.1029/2005GB002579.

- 633 Peterson, M.L., Thoreson, D.S., Hedges, J.I., Lee, C., Wakeham., S.G., 1993. Field evaluation  
634 of a valved sediment trap. *Limnol. Oceanogr.* 38, 1741-1761.
- 635 Peterson, M.L., Wakeham, S.G., Lee, C., Askea, M., Miquel, J.-C., 2005. Novel techniques for  
636 collection of sinking particles in the ocean and determining their settling rates. *Limnol.*  
637 *Oceanogr. Methods* 3, 520-532.
- 638 Peterson, M.L., Fabres, J., Wakeham, S.G., Lee, C., Miquel, J.-C. Sampling the vertical particle  
639 flux in the upper water column using a large diameter free-drifting NetTrap adapted to an  
640 Indented Rotating Sphere sediment trap (this volume)
- 641 Pilskaln, C.H., Lehmann, C., Paduan, J.B., Silver, M.W., 1998. Spatial and temporal dynamics in  
642 marine aggregate abundance, sinking rate and flux: Monterey Bay, central California.  
643 *Deep-Sea Res. II* 45, 1803-1837.
- 644 Ploug, H., Iversen, M.H., Koski, M., Buitenhuis, E.T., 2008. Production, oxygen respiration  
645 rates, and sinking velocity of copepod fecal pellets: Direct measurements of ballasting by  
646 opal and silicate. *Limnol. Oceanogr.* 53, 469-476.
- 647 Sarmiento J.L., Gruber, N. 2006. *Ocean biogeochemical dynamics*. Princeton Univ. Press,  
648 Princeton, NJ, USA.
- 649 Trull, T.W., Bray, S.G., Buesseler, K.O., Lamborg, C.H., Manganini, S., Moy, C., Valdes, J.,  
650 2008. In-situ measurement of mesopelagic particle sinking rates and the control of carbon  
651 transfer to the ocean interior during the Vertical Flux in the Global Ocean (VERTIGO)  
652 voyages in the North Pacific. *Deep-Sea Res. II* 55, 1684-1695.
- 653 Wakeham, S.G., Lee, C., Peterson, M.L., Liu, Z., Slozek, J., Putnam, I.F., Xue, J. Organic  
654 biomarkers in the twilight zone – time series and settling velocity sediment traps during  
655 MedFlux (this issue)
- 656 Xue, J., Armstrong, R.A. A new method for estimating settling velocities of sinking particles in  
657 the open ocean (this volume)
- 658
- 659
- 660
- 661
- 662
- 663

	2003				2005			
	cup#	t_open (min)	t_close (min)	SV_min (m/d)	cup#	t_open (min)	t_close (min)	SV_min (m/d)
669	1	(open during deployment/recovery)						
671	2	0	1	980	2	0	1	980
672	3	1	2	490	3	1	2	490
673					4	2	3	330
674	4	2	5	200	5	3	5	200
675					6	5	7	140
676	5	5	10	100	7	7	10	100
677	6	10	20	50	8	10	20	50
678	7	20	45	20	9	20	45	20
679	8	45	90	10	10	45	90	10
680	9	90	180	5	11	90	180	5
681	10	180	360	2.7				
682	11	360	720	1.4				
683	12	720	1440	0.7	12	180	1440	0.7

684

685

686 Table 1. Opening and closing times for collection cups in 2003 and 2005, and the minimum  
687 settling velocity associated with each interval. SV's have been rounded slightly to facilitate  
688 discussion; the "exact" value of the SV\_min are  $0.68 \text{ (m)} * 1440 \text{ (min/d)} / t_{\text{close}} \text{ (min)}$ . Given  
689 the observation in 2003 (Table 2) that peak fluxes occur at a closing time of about 3 minutes,  
690 timing was changed in 2005 to provide greater resolution at short closing times.

691

692

693

694

695

696

697

698

699

700

701	Deployment	SV1/2	<sup>a</sup> $\left(\overline{MF}_{total}\right)_{model}$	<sup>b</sup> $t_{mode}$	<sup>c</sup> $SV_{mode}$	<sup>d</sup> $\sigma_{Gauss}$	<sup>e</sup> $f_{Gauss}$	<sup>f</sup> $k_{slow}$
702	(year – depth)		(mg m <sup>-2</sup> d <sup>-1</sup> )	(min)	(m d <sup>-1</sup> )	( --- )	( --- )	(d <sup>-1</sup> )
703								
704								
705	Mar-May 2003	SV1	286	3.02	325	0.299	0.617	3.06
706		SV2	306	3.41	287	0.240	0.745	3.01
707		both	308	3.27	300	0.272	0.665	3.16
708								
709	May-Jun 2003	SV1+2	35	2.71	362	0.284	0.690	1.18
710								
711	2005 – 313m	SV2	480	3.30	297	0.311	0.665	4.68
712	2005 – 524m	SV1	476	1.95	503	0.277	0.654	4.76
713		SV2	547	3.11	315	0.360	0.726	3.51
714		both	536	2.54	386	0.341	0.688	4.50
715	2005 – 1918m	SV1	436	2.29	428	0.267	0.774	5.23
716		SV2	463	3.19	307	0.331	0.760	5.18
717		both	469	2.72	360	0.316	0.763	5.49
718								

719 <sup>a</sup> Estimated time-averaged mass flux during the deployment (mg m<sup>-2</sup> d<sup>-1</sup>)

720 <sup>b</sup> Estimated time at the mode of the Gaussian part of the fitted curve (min)

721 <sup>c</sup> Settling velocity at the peak of the Gaussian part of the fitted curve (m d<sup>-1</sup>)

722 <sup>d</sup> Standard deviation of the Gaussian part of the curve (dimensionless)

723 <sup>e</sup> Fraction of flux in the fast-sinking (Gaussian) fraction (dimensionless)

724 <sup>f</sup> Decay constant of the slow-sinking (exponential) fraction (d<sup>-1</sup>)

725

726

727 Table 2. Parameter values for sinking velocity spectra modeled as the sum of a Gaussian curve

728 for fast-settling particles plus exponential settling of slow-sinking particles. Here, roman type

729 denotes parameters from individual traps on multiple-trap arrays, and italic type denotes either

730 single traps or simultaneous fits to paired traps on the same array; the latter were used to

731 generate the fitted curves in Figs. 1 and 2. The notations “SV1” and “SV2” refer to two SV traps  
732 on the same frame; “both” refers to parameters from a simultaneous fit to data from SV1 and  
733 SV2; and “SV1+2” in May-June 2003 is a case where samples from both traps were combined  
734 before chemical analysis because the individual samples were very small. Note that the values of  
735  $\left(\overline{MF}_{total}\right)_{model}$  were estimated by curve fitting; they are not the measured quantities  
736  $\left(\overline{MF}_{total}\right)_{data}$ . Estimating the values of  $\left(\overline{MF}_{total}\right)_{model}$  preserves the statistical independence of  
737 the individual cup mass measurements, and allows simpler interpretation of the fits; their values  
738 were always within a few percent of measured values  $\left(\overline{MF}_{total}\right)_{data}$ .

739  
740  
741  
742  
743  
744  
745  
746  
747  
748  
749  
750  
751  
752  
753  
754  
755  
756  
757  
758  
759  
760

761	Deployment	SV1/2	$\left(\overline{MF}_{total}\right)_{model}$	$SV_{mode}$	$SV_{mean}$
762	(year – depth)		( $\text{mg m}^{-2} \text{d}^{-1}$ )	( $\text{m d}^{-1}$ )	( $\text{m d}^{-1}$ )
763					
764					
765	Mar-May 2003 – 238m	SV1	286	325	238
766		SV2	306	287	214
767					
768	May-Jun 2003 – 117m	SV1+2	35	362	237
769					
770	Feb-Apr 2005 – 313m	SV2	480	297	219
771	Feb-Apr 2005 – 524m	SV1	476	503	298
772		SV2	547	315	224
773	Feb-Apr 2005 – 1918m	SV1	436	428	280
774		SV2	463	307	224
775					
776	Averages			$353 \pm 76$	$242 \pm 31$

777

778 Table 3. Comparison of modal and mean sinking velocities (and their standard deviations) for the

779 eight SV traps in MedFlux. Mean SV's were calculated using only SV classes > 50 m/d, the

780 location of the transition point between the Gaussian section and the exponential section in Figs.

781 1 and 2: therefore, in 2003, cups 2 – 6 were included in the average, and in 2005, cups 2 – 8.

782

783

784

785

786

787

788

789

790

791

792

## Figure Legends

793  
794  
795

796 Figure 1. Histograms of time-averaged mass flux density, normalized to a collection area of 1  
797  $\text{m}^2$ , versus sinking velocity (m/d), for deployments in 2003. The area of histogram  
798 element  $i$  represents the mass caught in Settling Velocity Interval (SVI)  $i$  over the  
799 deployment period ( $\text{mg}/\text{m}^2/\text{d}$ ); the total area under each histogram represents total mass.  
800 The heights of each histogram element (units:  $\text{mg}/\text{m}^2/\text{d}/\text{SVI}$ ) represent the intensity of  
801 the settling process in a given SV class, and so are directly comparable to the heights of  
802 the continuous model (Gaussian + exponential curves) that was fit to the data; see text,  
803 especially section 2.2, for further details. a) 6 March - 6 May 2003 (61 d), 238 m; b) 14  
804 May - 30 June 2003 (47 d), 117 m.

805 Figure 2. Histograms of time-averaged mass flux density ( $\text{mg}/\text{m}^2/\text{d}/\text{SVI}$ ) versus sinking velocity  
806 (m/d) for deployments in 2005. All deployments were 4 March – 1 May 2005 (55 d). a)  
807 313 m; b) 524 m; c) 1918 m. See the legend to Fig. 1 for further details.

808 Figure 3. Calculated mass concentration densities  $\overline{MCD}_i$  ( $\text{mg}/\text{m}^3/\text{SVI}$ ) outside the trap versus  
809 settling velocities  $SV_i$  (m/d). Note that these densities, whose ratios represent ratios of  
810 mass densities corrected to equal SVI (see Section 2.2), span over 4 orders of magnitude,  
811 with slower SV classes being much more abundant. The one curve that does not bunch  
812 with the others is that for May-June 2003, whose mass flux densities were an order of  
813 magnitude smaller than those of other collections.

814 Figure 4. Average settling velocity (m/d) versus minimum settling velocity (m/d) included in the  
815 average. (See section 2.4, especially Eq. 14).

816 Figure 5. Mass flux density in each SV interval normalized to total mass flux (final units:  
817  $\text{SVI}^{-1}$ ), plotted versus sinking velocity (m/d), for all Medflux deployments. This  
818 normalization allows the shapes of the data spectra to be compared without the  
819 distraction of total flux. Each line represents data from one trap in Fig. 1 or 2; the  $x$ -  
820 coordinate of each point is the midpoint of an SV interval, and the  $y$ -coordinate is the  
821 height of the corresponding histogram element.

822 Figure 6. Mass flux density in each SV interval normalized to unit total mass flux ( $\text{SVI}^{-1}$ ),  
823 plotted versus sinking velocity (m/d), for the deployments plotted in Fig. 4 of Trull et al.

824 (2008) and from MedFlux. Shown are data from their shallow deployments at stations  
825 ALOHA (272 m) and K2 (281 m and 285 m; see their Table 3), along with data from  
826 three MedFlux traps at comparable depths (March-May 2003, SV1 and SV2, 238 m; and  
827 Feb-April 2005, SV2, 313 m). ALOHA and K2 data have been replotted as described in  
828 Section 2.2 to allow direct comparison between data sets. See the legend to Fig. 5 for  
829 further details.  
830

Figure 1a (March - May 2005, 238m)

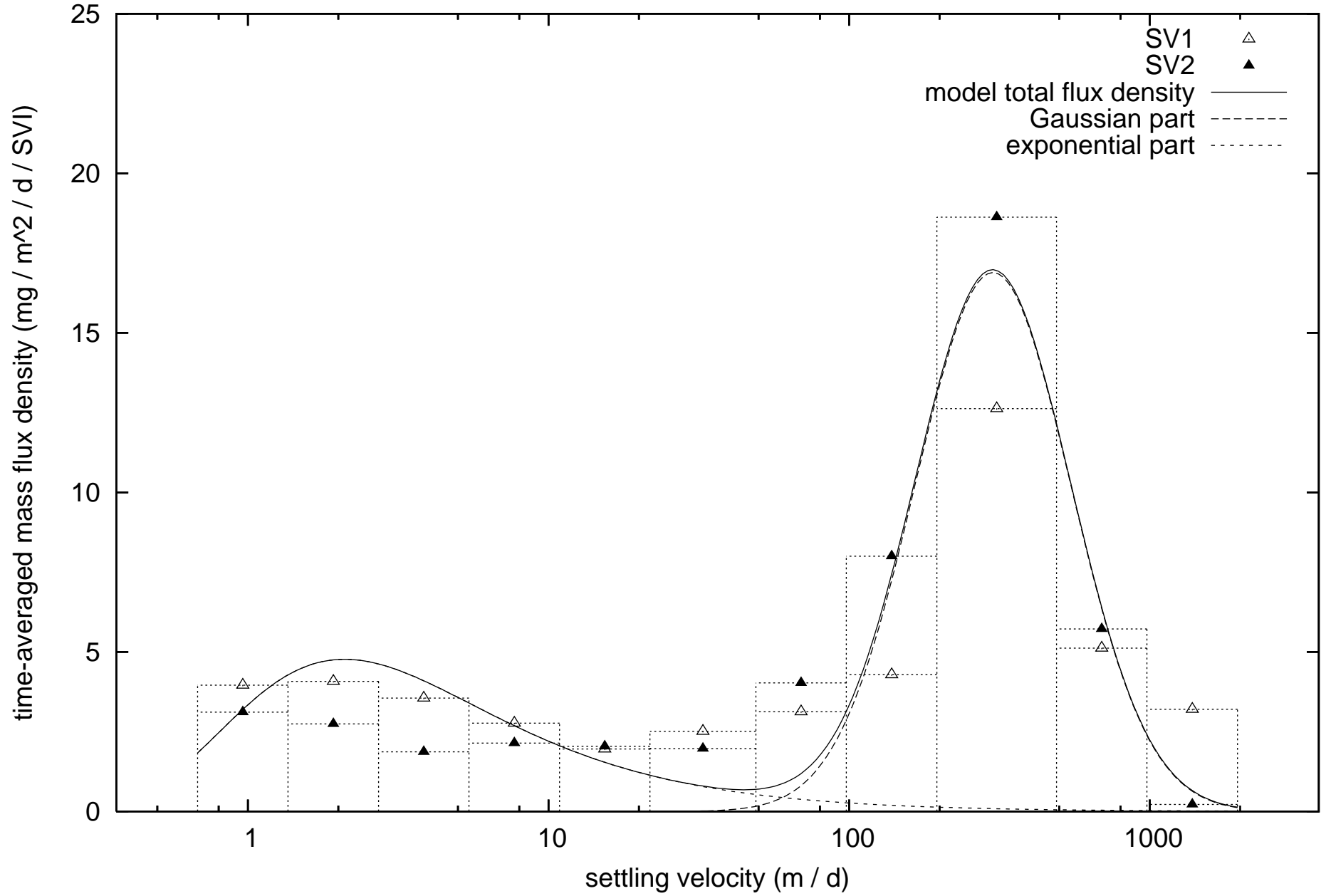


Figure 1b (May - June 2003, 117m)

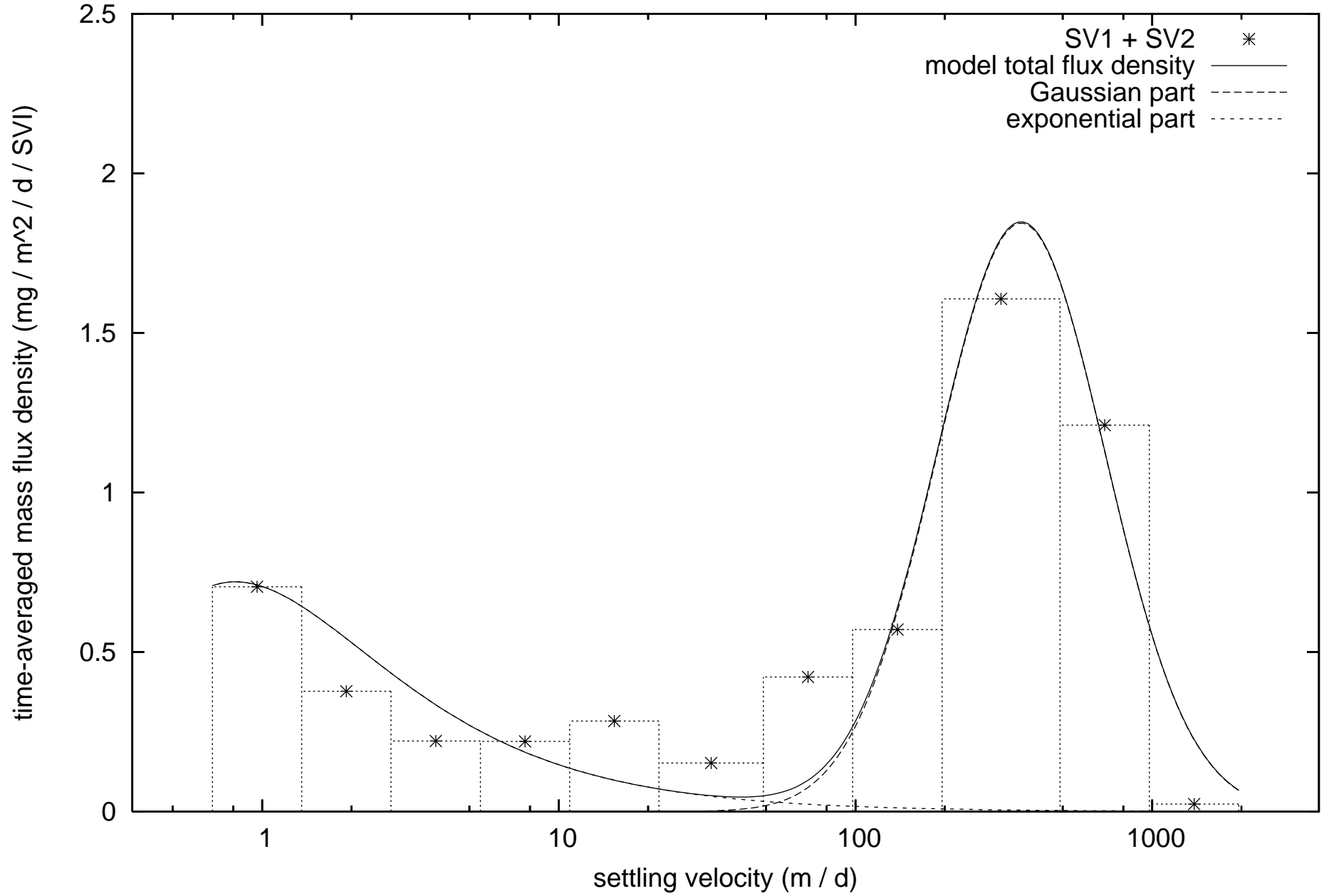


Figure 2a (February - April 2005, 313m)

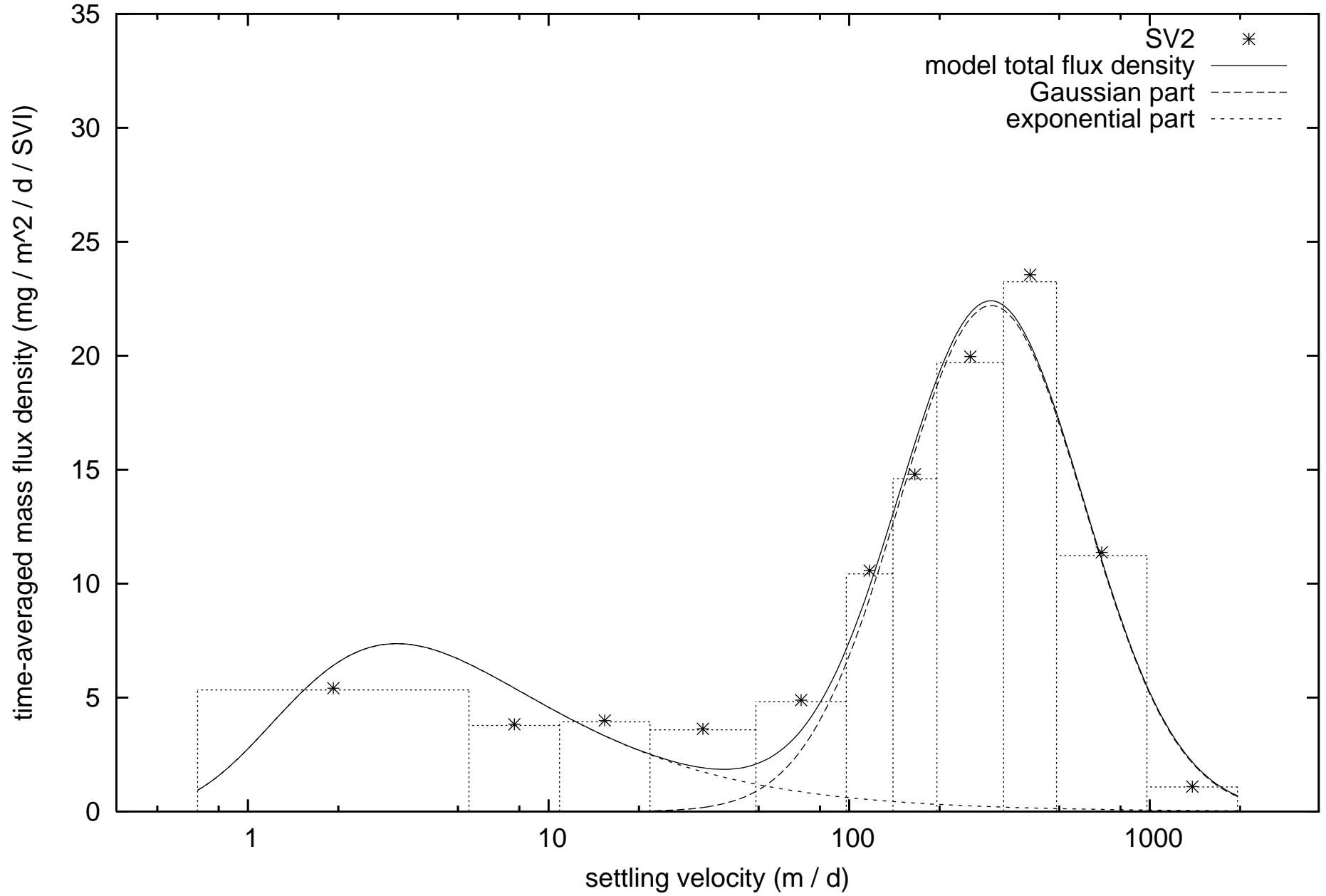


Figure 2b (February - April 2005, 524m)

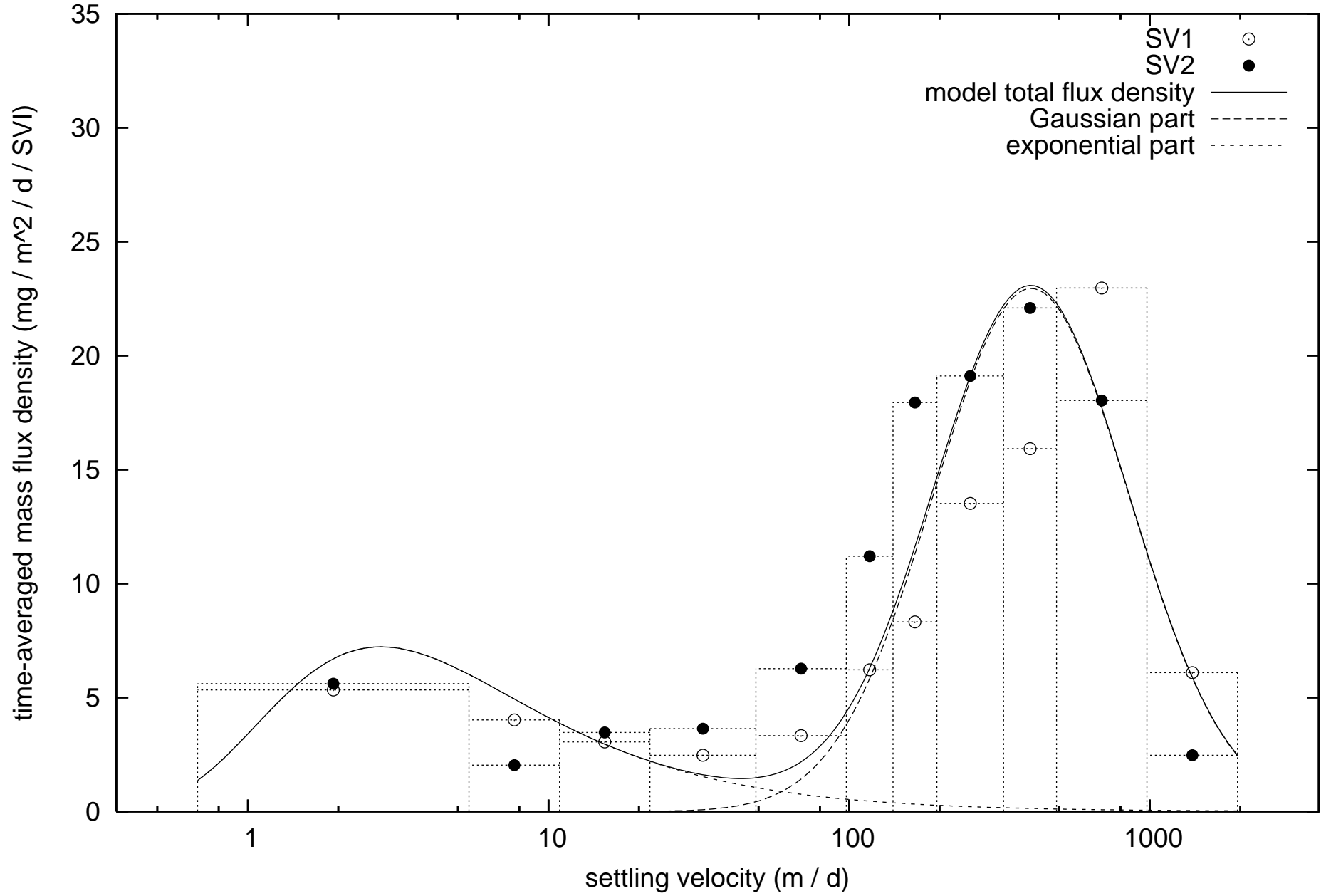


Figure 2c (February - April 2005, 1918m)

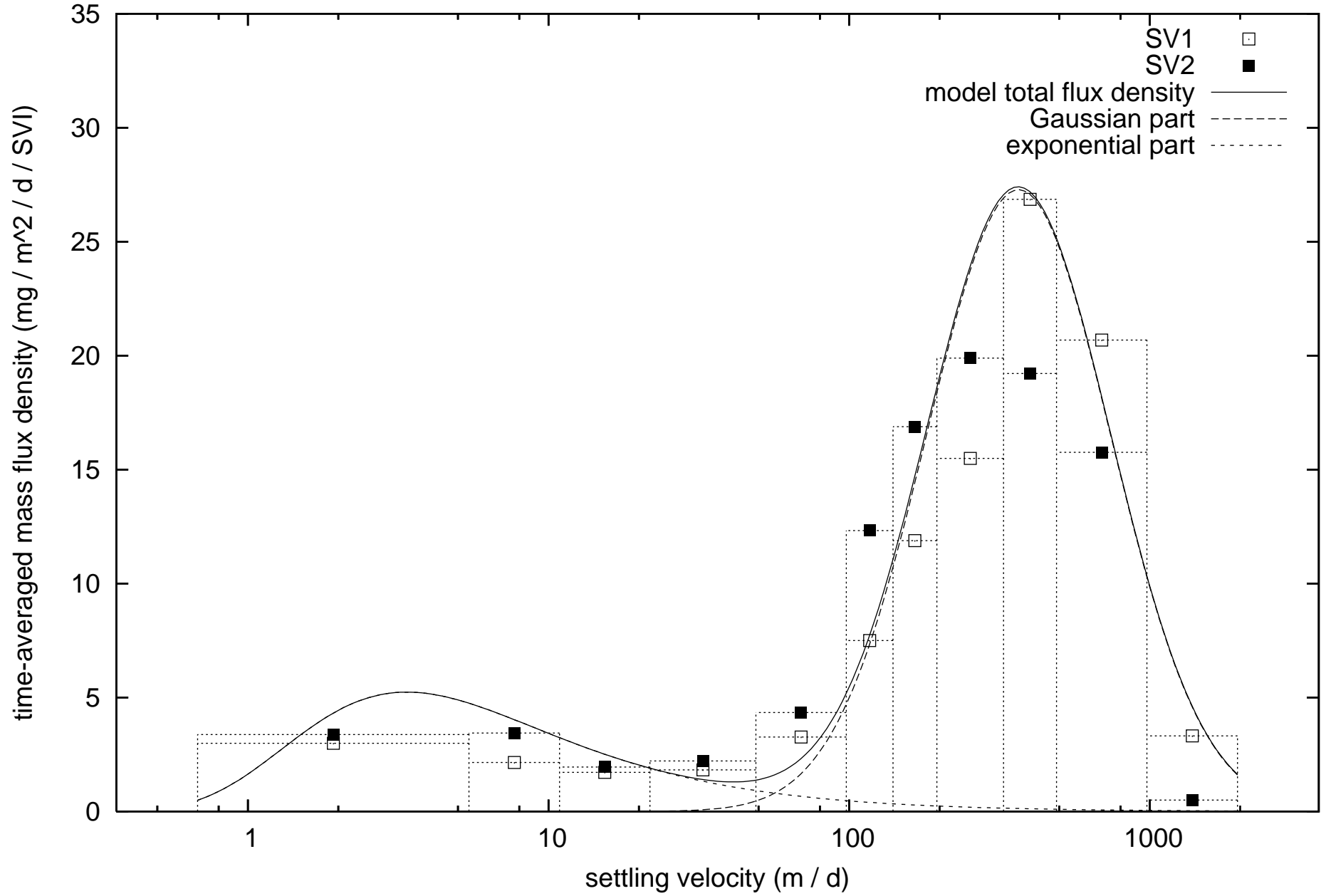


Figure 3: all MedFlux data

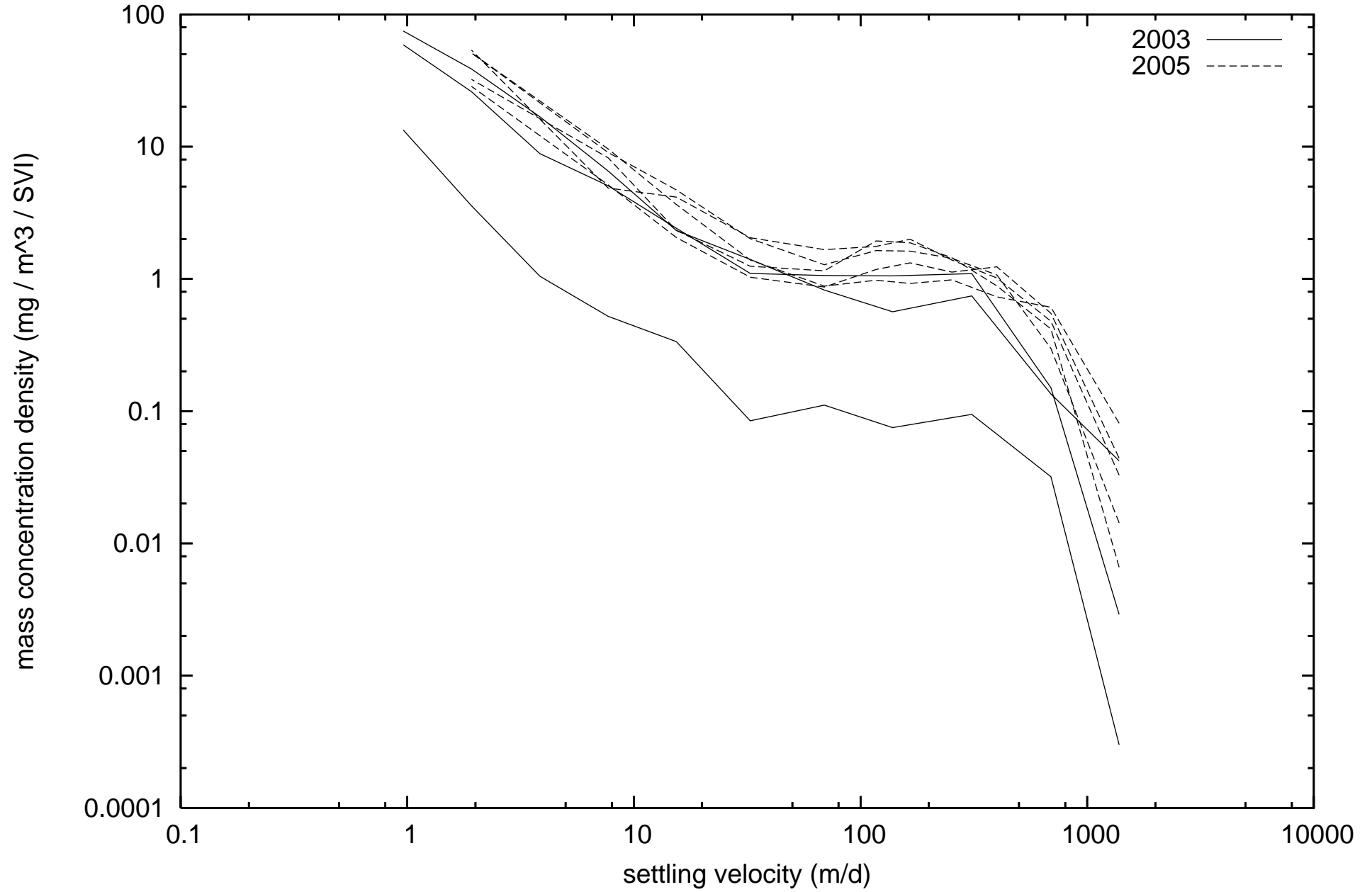


Figure 4

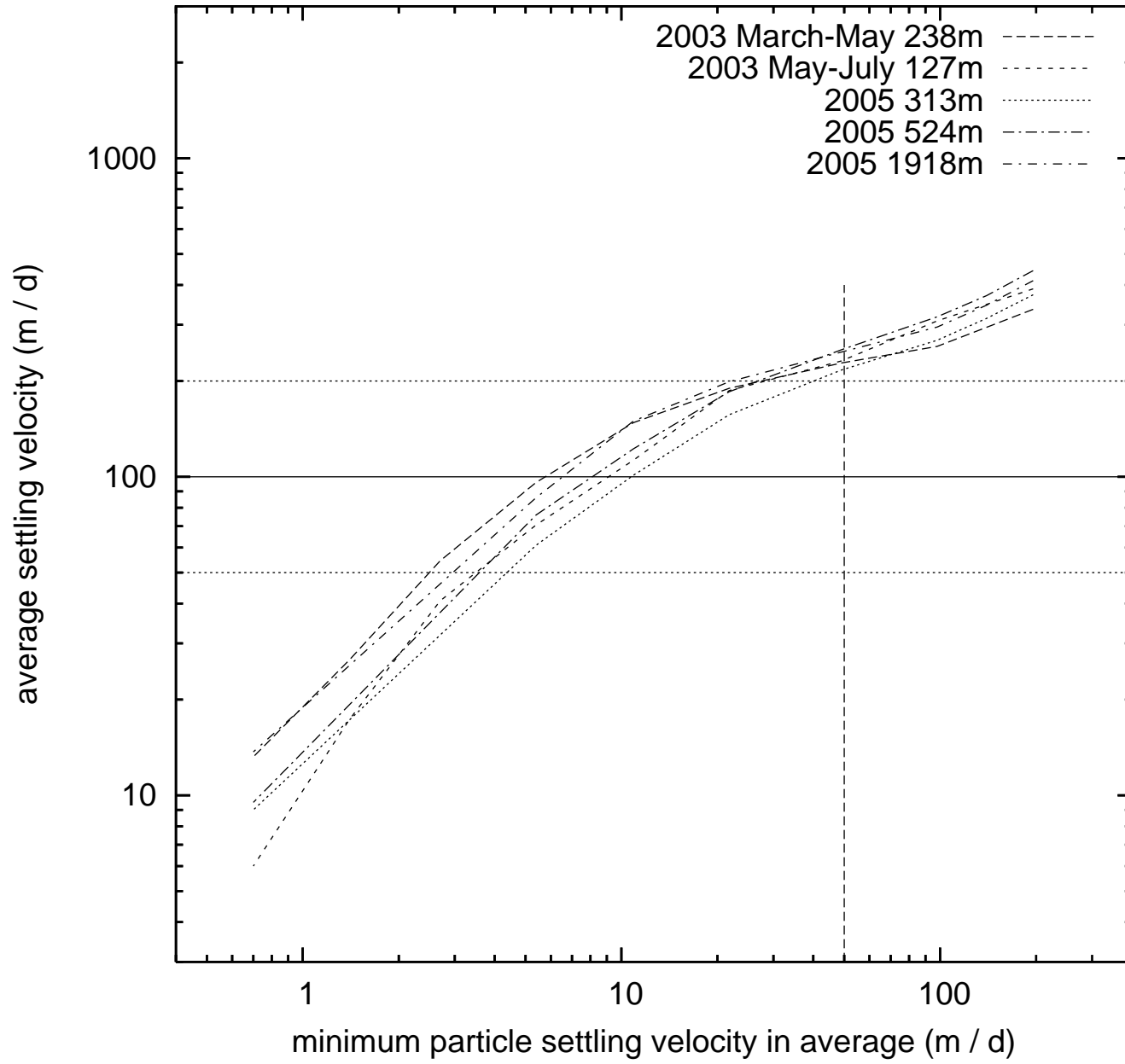


Figure 5: all MedFlux data

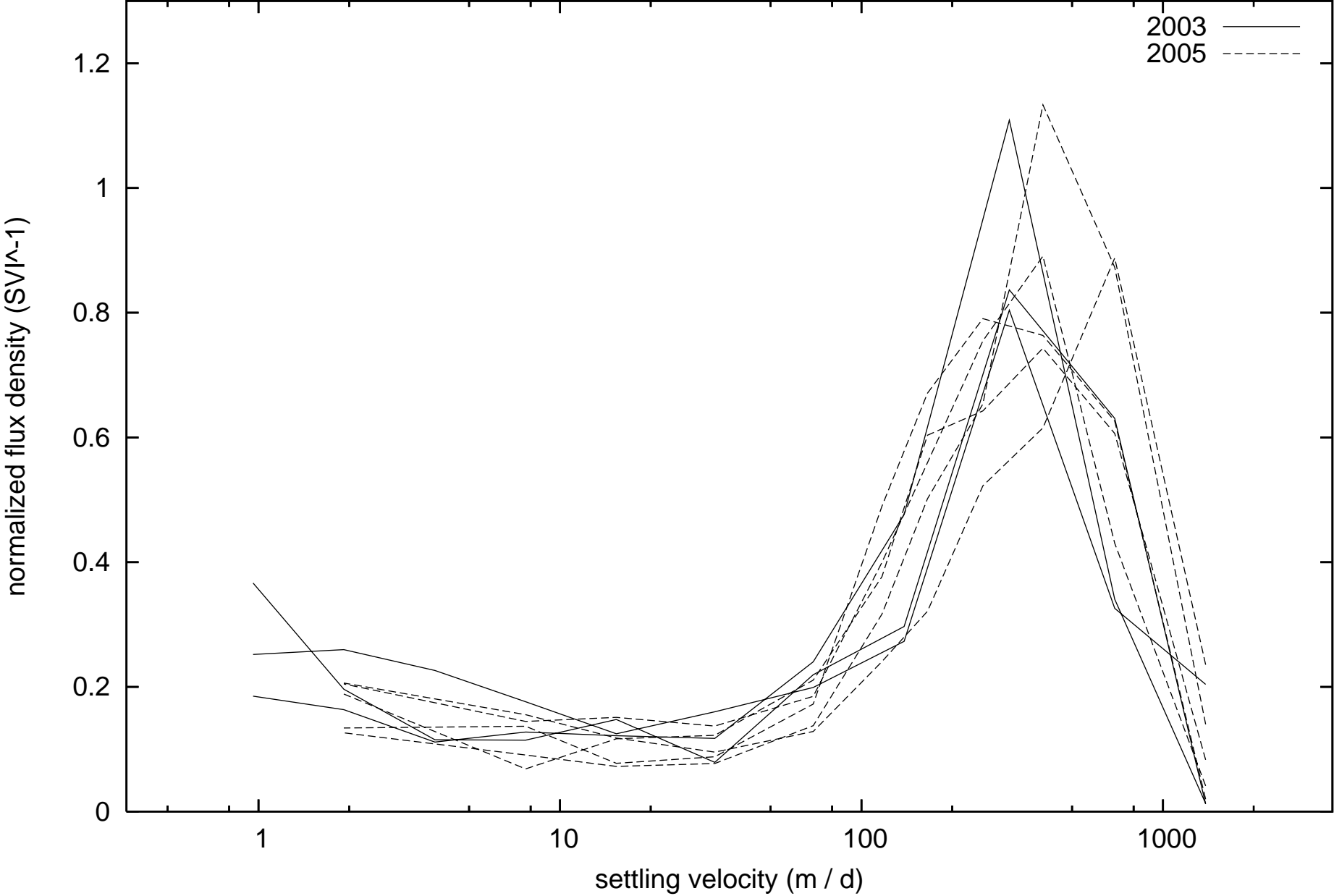


Figure 6: VERTIGO data compared to Medflux data

